Hindawi
Complexity
Volume 2020, Article ID 6161784, 17 pages
https://doi.org/10.1155/2020/6161784

Research Article

Characteristic Analysis and Optimal Regulation of Primary Frequency Regulation Condition in Low Water Head Area Based on Hydraulic-Mechanical-Electrical Coupling Model of Pumped Storage Unit

Cong Lv,[1] Yanhe Xu ,[1] Xin Wu,[1] and Qing Zhang[2]

[1]*School of Hydropower and Information Engineering, Huazhong University of Science and Technology, Wuhan 430074, China*
[2]*Nondestructive Detection and Monitoring Technology for High Speed Transportation Facilities, Key Laboratory of Ministry of Industry and Information Technology, Nanjing 210016, China*

Correspondence should be addressed to Yanhe Xu; yh_xu@hust.edu.cn

Received 8 September 2019; Revised 19 November 2019; Accepted 7 December 2019; Published 11 January 2020

Academic Editor: Marcin Mrugalski

Pumped storage power station is an important regulating tool for peak load regulation and frequency regulation of the power grid, especially its primary frequency regulation function, which is of profound significance for the safety and stability of the power grid. As the core equipment of the pumped storage power station, the reversible design of the pump turbine makes it easy to have hydraulic fluctuation and mechanical instability when the unit runs to the "S" characteristic area, which will cause the frequency oscillation of the generator under the condition of primary frequency regulation. Therefore, some innovative work is studied in this paper: (1) an accurate hydraulic-mechanical-electrical coupling system mathematical model of pumped storage unit regulation system (PSURS) is established based on full characteristic curve of the pump turbine and seventh-order synchronous generator and excitation system; (2) the dynamic response characteristics of primary frequency regulation of pumped storage unit (PSU) under different water heads and different frequency disturbances are analyzed by numerical simulation; (3) in view of the unstable condition of the unit under the large frequency disturbance when it operates in the low head and small load area, the objective optimization function considering the ITAE index of hydraulic, mechanical, and electrical factors is proposed; and (4) fractional-order PID controller and the bacterial-foraging chemotaxis gravitational search algorithm (BCGSA) combined optimization strategy is used for PSURS optimization regulation and parameter optimization. The results show that the joint optimization strategy proposed in this paper has smaller objective function value, and makes the PSURS pass through the unbalanced area quickly, with better primary frequency regulation speed and smaller regulation depth.

1. Introduction

In recent years, with the rapid growth of China's power load, the demand for the stability of the power grid is rapidly increasing, and the shortage of peak load regulation capacity has become an important problem restricting the development of the power system. Therefore, the combined operation of pumped storage technology and new energy is widely used in power system [1, 2]. Pumped storage power station is mainly responsible for peak and frequency regulation and peak and valley cutting, which can improve the power supply quality, flexibility, and reliability of the power grid and enable various power resources to be reasonably applied, which is an important part of the power system [3]. The pumped storage power station is dedicated to power management and stability regulation of grid and isolated power system [4].

The frequency regulation function of PSU is very important to maintain the stability of power grid frequency, especially for those power grids with small proportion of prompt adjustment units [5]. An et al. proposed an improved frequency dead zone with feed-forward control to

optimize the frequency regulation function of PSU [6]. Yang and Yang and Zhao and Ren also studied the role of pumped storage units in enhancing power system stability and frequency control [7, 8]. It can be seen from some accidents in the power system that the units with the input of primary frequency regulation function and the correct setting of primary frequency regulation parameters can greatly restrain the expansion of the accident and ensure the stability of the power system [9–11]. The pumped storage unit regulation system (PSURS) has strong nonlinear and time-varying characteristics [12], and PSU has "S" characteristic area, which leads to the frequency oscillation of the unit under low water head [13, 14]. Therefore, it is of profound significance to optimize the dynamic performance and control quality of PSURS under the condition of low water head [15].

At present, PID controller is widely used as controller in hydraulic turbine regulating system due to its good control effect, simple and easy to implement structure, strong robustness, and other advantages [16, 17]. However, when the PSURS is running at a low water head, it is easy to enter the "S" characteristic area, resulting in widespread range fluctuation and unstable operation of the unit's frequency. Especially when the unit participates in primary frequency regulation [18], the frequency disturbance will greatly increase the probability of wide range fluctuation of the PSU's frequency. The traditional PID controller cannot adjust the frequency fluctuation of PSU well. In recent years, FOPID controller has been used in a lot of research studies [19, 20]. Xu et al. designed an adaptive fast fuzzy fractional-order PID controller to improve the dynamic performance of pumped storage units under low water head no-load condition [21]. Chen et al. designed a fractional-order PID controller for hydraulic turbine regulating system [22]. Tang et al. designed a fractional-order controller for automatic voltage regulator [23]. Zhang et al. optimized the FOPID controller of PSURS under multiple working conditions [24]; the common first-order generator model has been applied, and electrical factors such as active power, voltage, current, and excitation regulation system have not been considered deeply. Compared with traditional PID controller, the FOPID controller has two more adjustable parameters, which improve its control performance. However, at the same time, additional two adjustable parameters also make the optimal setting of fractional PID controller parameters more difficult [25].

Many excellent intelligent optimization algorithms are widely used in parameter optimization of PSU at present [26]. Malik and Zeng proposed a method for parameter optimization of PID governor of hydraulic turbine generator set based on the algorithm of bacteria-particle swarm optimization [27]. Lai et al. used the artificial flock algorithm to optimize the control of PSU [28]. Zhang et al. proposed a novel chaotic grey wolf optimization algorithm to select the optimal control parameters of the pump turbine governing system [29]. Gravitational search algorithm (GSA) is a new intelligent optimization algorithm proposed by Rashedi et al. [30]. It has strong global searching ability and convergence speed and is more effective in PID parameter setting. Premature and falling into local optimum are two common shortcomings of GSA and other swarm intelligence algorithms, which will reduce the accuracy and efficiency of algorithm optimization [31]. Xu et al. proposed a bacterial-foraging chemotaxis gravitational search algorithm (BCGSA) which can effectively improve these problems [21].

Accurate model is essential to optimal regulation and control research. Nonlinear structural model of pump turbine based on the characteristic curve can better describe nonlinear hydraulic and mechanical characteristics. The model of seventh-order synchronous generator fully considers electromagnetic transient and subtransient processes and can better respond to frequency changes [32]. Therefore, this paper puts forward an accurate hydraulic-mechanical-electrical fine coupling system mathematical model of PSURS based on and high-order synchronous generator and full characteristic curve of pump turbine. Moreover, the primary frequency regulation characteristics of the PSURS are tested by numerical simulation. The results show that it is easy to enter the unstable area and cause a violent oscillation of the PSURS under the condition of low water head, small load, and large frequency disturbance. Choosing a suitable optimal control method is still an important and challenging issue for this unstable condition. So, the FOPID controller with BCGSA is adopted during frequent disturbance process of +0.5 Hz and −0.5 Hz under low water head and small load condition.

The remainder of the paper is structured as follows. Section 2 establishes the hydraulic-mechanical-electrical coupling model of pumped storage unit regulation system. Section 3 proposes frequency regulation performance analysis of pumped storage units with different water heads and loads. Section 4 describes the optimization method of control parameters including FOPID and BCGSA. Section 5 discusses the experimental results, and Section 6 summarizes the conclusion of the research.

2. Hydraulic-Mechanical-Electrical Coupling Model

PSURS is a complex closed-loop control system which includes the material and energy exchange of hydraulic, mechanical, and electrical factors which is composed of a water diversion system [33], pump turbine, synchronous generator, excitation system, and governor, as shown in Figure 1.

2.1. Model of Water Diversion System. In the modeling of PSUSRS, the water diversion system is usually reduced to a section of equivalent pipe and modeled by water hammer theory. Equivalent simplified models of water diversion system can be divided into rigid water hammer models, approximate elastic water hammer models, and elastic water hammer models. In this paper, the primary frequency regulation condition is small fluctuation condition, and the hydraulic fluctuation is minor variation. Considering the simulation accuracy and hydraulic calculation efficiency, an approximate elastic water hammer model is adopted, and its transfer function is shown in the following equation [34]:

$$G_h(s) = -h_w \frac{T_r s}{1 + (1/2) f T_r s + (1/8) T_r^2 s^2}. \quad (1)$$

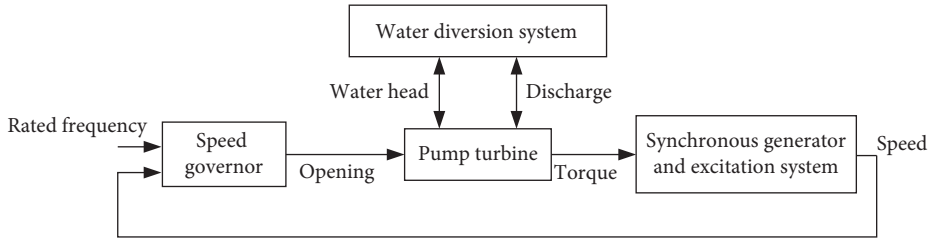

Figure 1: Structure of PSURS.

2.2. Model of Pump Turbine. Pump turbine is the key component of PSURS, and there is no accurate analytic expression to describe the dynamic characteristics of this system until now. The flow and torque characteristics of the pump turbine are complex. It is even impossible to obtain the accurately analytic expression of the pump turbine. Through the model experiment, the comprehensive characteristic curve of the pump turbine and the steady-state characteristics of the pump turbine like the pump turbine flow and torque characteristics can be achieved. The instantaneous parameters of the unit are calculated by the characteristic curve, and the dynamic characteristics are obtained.

At present, mathematical modeling of the pump turbine mainly includes linear analytical model, internal characteristic model, and interpolation model based on full characteristic curve. The hydraulic-mechanical-electrical coupling model should be able to describe the dynamic characteristics of the process of converting water energy into rotating mechanical energy, so interpolation model based on full characteristic curve is adopted in this paper [21]. The characteristic curve of the pump turbine takes the true value of the guide vane opening y as parameter to establish the flow characteristic curve Q_{11}~N_{11} and torque characteristic curve M_{11}~N_{11} of the pump turbine, as shown in the following equation [35]:

$$\begin{cases} Q_{11} = Q_{11}(y, N_{11}), \\ M_{11} = M_{11}(y, N_{11}). \end{cases} \tag{2}$$

Due to the "S" area of the characteristic curve of the pump turbine, the problem of "one input and many outputs" exists in the interpolation calculation. The logarithmic curve projection (LCP) method not only solves the multivalue problem of zero opening degree, small opening degree, and "S" characteristic region of guide vane opening in the description of runner characteristics but also facilitates the solution and has high precision. The LCP is described as follows [36]:

$$n_1 = \frac{N_{11}}{N_{11r}}, \tag{3}$$

$$v_1 = \frac{Q_{11}}{Q_{11r}}, \tag{4}$$

$$m_1 = \frac{M_{11}}{M_{11r}}, \tag{5}$$

$$x = \frac{n_1}{e^{v1}}, \tag{6}$$

where Q_{11r}, N_{11r}, and M_{11r} are rated unit flow, rated unit rotational speed, and rated unit torque.

Characteristic curved surfaces obtained by LCP are shown in Figure 2. The flow Q_{11t} and torque M_{11t} calculation process of the pump turbine mathematical model is summarized as the following:

Step (1): Initialization. Initialize the guide opening y_t and unit rotational speed n_{11t} at t time and unit flow $Q_{11t-\Delta t}$ at $t - \Delta t$ time.

Step (2): Transformation. Let $Q_{11t}^{(0)} = Q_{11t-\Delta t}$ and calculate the abscissa $x_t^{(n)}$ using transform formulas (3)–(6) of LCP.

Step (3): Interpolation. For curves $x - Q_{11}$ and $x - M_{11}$ of Figure 2, calculate $M_{11t}^{(n)}$ and $Q_{11t}^{(n)}$ using y_t and $x_t^{(n)}$ as inputs by the interpolation method.

Step (4). Calculate absolute value error of $Q_{11t}^{(n+1)}$ and $Q_{11t}^{(n)}$, while n changes from 1 to N_{iter}. If $|Q_{11t}^{(n+1)} - Q_{11t}^{(n)}| < \sigma$, directly output Q_{11t} and M_{11t}; else update $Q_{11t}^{(n+1)}$ by $Q_{11t}^{(n+1)} = Q_{11t}^{(n)} - \tau \cdot |Q_{11t}^{(n)} - Q_{11t}^{(n-1)}|$, where τ is the scale factor and σ is the calculation accuracy coefficient.

Step (5): Iterative Calculation. Repeat Step (2) to Step (4) until the stop criteria reached. When $n = N_{\text{iter}}$ and the stop criteria are not reached, if $|Q_{11t}^{(n+1)} - Q_{11t}^{(n)}| \le 10\sigma$, directly output Q_{11t} and M_{11t}; else output values according to the given formulas $Q_{11t} = Q_{11t}^{(n)} + 5\sigma$ and $M_{11t} = M_{11t}^{(n)} + 5\sigma$.

2.3. Model of Synchronous Generator. Synchronous generator is the core of the power system. Its dynamic performance is very complex. In the mathematical model of synchronous motors, the zero shaft winding is not considered. The electromagnetic transition process of the five windings d, q, f, D, and Q (winding flux or current as the state variable) and the rotor mechanical transition process (δ, ω as the state variable) constitute the synchronous motor as a seventh-order model [32, 37]. In this paper, the combined transition process of water and electricity is studied. Considering the electromagnetic transient and subtransient processes, the seventh-order generator model is selected.

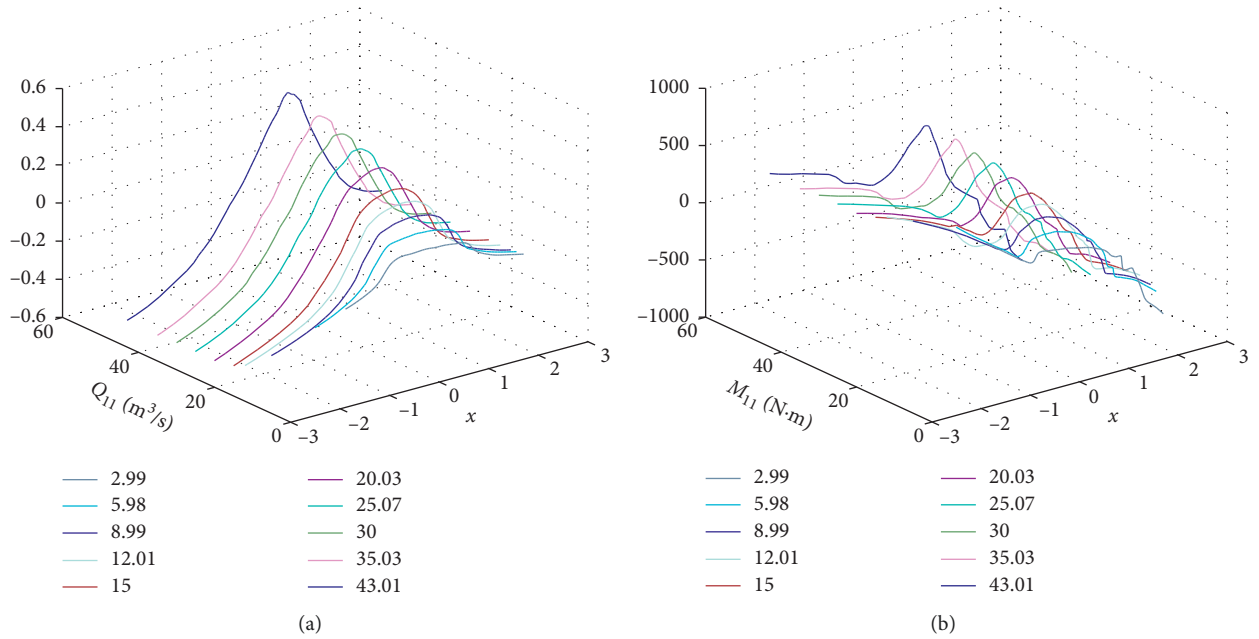

Figure 2: Logarithmic curve projection of the characteristic curves.

The voltage equation of each winding of the synchronous motor is shown in the following equation (Park equation) [38]:

$$\begin{cases} v_d = -r_a i_d + \dot{\psi}_d - \omega\psi_q, \\ v_d = -r_a i_q + \dot{\psi}_q - \omega\psi_d, \\ v_f = r_f i_f + \dot{\psi}_f, \\ v_D = 0 = r_D i_D + \dot{\psi}_D, \\ v_Q = 0 = r_Q i_Q + \dot{\psi}_Q, \end{cases} \tag{7}$$

where the subscript d represents the d axis winding, the subscript q represents the q axis winding, the subscript f represents the rotor excitation winding, the subscript D represents the d axis equivalent damping winding, and the subscript Q represents the q axis equivalent damping winding.

The flux linkage equation of axis d and axis q reflects the magnetic coupling relationship between stator winding and rotor winding. The specific equation is shown in the following equation:

$$\begin{cases} \psi_d = -x_d i_d + x_{ad}\left(i_f + i_D\right), \\ \psi_q = -x_q i_q + x_{aq} i_Q, \\ \psi_f = x_f i_f + x_{ad}\left(i_D - i_d\right), \\ \psi_D = x_D i_D + x_{ad}\left(i_f - i_d\right), \\ \psi_Q = x_Q i_Q - x_{aq} i_q. \end{cases} \tag{8}$$

The rotor motion equation is shown in the following equation [39, 40]:

$$\begin{cases} \dfrac{\mathrm{d}\delta}{\mathrm{d}t} = (\omega - 1)\omega_0, \\ \dfrac{\mathrm{d}\omega}{\mathrm{d}t} = \dfrac{\left[T_m - \left(\psi_d i_q - \psi_q i_d\right)\right]}{2H}. \end{cases} \tag{9}$$

The second-order model of the generator rotor and the relationship between generator inertia and output power and power angle are considered, and the relationship between power angle and rotation speed is established. The second-order model of the rotor and the voltage equation of equation (7) constitute the seventh-order model of the generator.

2.4. Model of Excitation System. The excitation system provides the excitation power to the generator, acts as regulating the voltage, keeping the voltage at the end of the generator or the pivot point constant, and can control the reactive power distribution of parallel running generators. It can improve the stability limit of the power system and greatly improve the transient stability of the power system.

There are various kinds of excitation systems for synchronous generators. Different excitation models can be chosen according to the excitation mode of the hydropower station. The transient limiter is used in IEEE *ST1A* model, and the intrinsic excitation time constant is very small, so the stability of the excitation system can be ignored. Because this paper focuses on the dynamic stability of generator output frequency under the condition of primary frequency regulation, the stability of the excitation system can be ignored. So, this paper adopts the international standard IEEE *ST1A* excitation system model [41].

2.5. Model of Speed Governor. Microcomputer speed governor is commonly used in the speed control of the pump turbine in modern pumped storage power station. The speed governor is comprised of a microcomputer regulator and electro-hydraulic follow-up device. Currently, the widely used microcomputer regulator adopts the parallel PID

controller shown in Figure 3, and its transfer function is shown in the following equation:

$$G_{\mathrm{PID}}(s) = \left(K_p + \frac{K_d s}{T_d s + 1} + \frac{K_i}{s}\right)(n_{\mathrm{ref}} - n) + b_p(y_{\mathrm{ref}} - y). \tag{10}$$

Electro-hydraulic actuator is the actuator of the governor. The servo mechanism and the main valve of actuator can be described by two first-order inertia links in series. The transfer function of the electro-hydraulic actuator is shown in the following equation:

$$G(s) = \frac{k_0}{T_{yB}s + 1} \times \frac{1}{T_y s}. \tag{11}$$

The purpose of PSURS optimization is to suppress the instability of various operating conditions and make the system safe and stable. To accurately reflect the strong nonlinearity of the regulation system of PSU under the coupling of hydraulic, mechanical, and electrical factors, the nonlinear model structure of the regulation system was adopted in this paper, as shown in Figure 4.

3. Primary Frequency Regulation Performance Analysis

The primary frequency regulation function of PSU is very important to maintain the stability of power grid frequency, which can provide power support rapidly when the power grid suddenly changes in large load, improve the reliability of power system, optimize system dispatching, and stabilize the power grid frequency [42]. In order to study the dynamic regulation process of PSURS, the simulation experiment is performed in this section. The refined mathematical model of the regulation system of the pumped storage unit is shown in Section 2. The model of the pump turbine uses the data of the actual unit of a pumped storage power station in China. The water head and model parameters of the power station are shown in Table 1.

The control parameters $K_p = 3$, $K_i = 2$, and $K_d = 4$ are used to analyze the dynamic characteristics of the system when the PSURS receives frequency disturbances of 0.2 Hz and 0.5 Hz at different water heads with different loads. In this paper, the maximum opening of the pump turbine $y_{\max}$ is 43.1°, and the setting opening under different guide vane opening and different loads during the experimental analysis is shown in Table 2. The time domain performance analysis indicator is integral of time multiplied absolute error (ITAE). ITAE values of frequency f and guide vane opening y under various working conditions are shown in Tables 3–6. For convenience of comparison, data in the table are normalized. By these Tables, it is shown that under the same water head, the lower the unit with the load, the greater the ITAE_f (the ITAE value of the frequency) and the ITAE_y (the ITAE value of the opening),whether it has big frequency disturbance ($\Delta f = -0.5$ Hz) or small frequency disturbance ($\Delta f = -0.2$ Hz). If the ITAE value is relatively large, then the system is easier to instability and dynamic characteristics is worse, especially as $\Delta f = -0.5$ Hz. The ITAE_f and ITAE_y with 25% load are much higher than the value with greater load. At the same time, under the same load, when $\Delta f = -0.2$ Hz, ITAE value also increases slowly with the increase of water head. But when $\Delta f = -0.5$ Hz, the ITAE values of low water head ($H_w = 190$ m) with 25% load and 50% load are larger than other water head, and the instability degree is higher at 25% load.

After analysis of water head and frequency, the comprehensive ITAE index was set up as shown in equation (12), and its specific value and change trend are shown in Tables 7 and 8 and Figure 5. According to Figures 5(a) and 5(b), when the unit is carrying 25% load, the PSU is more likely to enter into an unstable state after frequency disturbance, and its performance is worse, especially under low water head ($H_w = 190$ m) and large $\Delta f = -0.5$ Hz.

Figure 6 shows the comparison between low water head $H_w = 190$ m and high water head ($H_w = 210$ m) of guide vane opening y, water hammer pressure h, and dynamic PE under different loads. Comparative analysis shows that the lower the load, the worse the dynamic characteristics of the system. At 25% load, the PSURS experienced violent oscillation, and when $H_w = 190$ m, the amplitude of oscillation was larger, especially violent.

By analyzing the simulation experiment of frequency disturbance of the regulating system with different water heads and different load conditions, it can be known that PSURS is easy to enter the unstable area and cause violent oscillation of the system under the condition of low water head, small load, and large frequency disturbance. At this time, the control capability of the PSURS is required to increase, and appropriate control strategies and parameters are particularly important to maintain the stability of the frequency of the units and the power grid.

4. Control Parameter Optimization Method

4.1. Fractional-Order PID Controller. The fractional-order PID controller is denoted as $\mathrm{PI}^{\lambda}\mathrm{D}^{\mu}$ [22]. It is a generalization of classical integer-order controller, which is more concise and accurate for complex practical systems [43]. Due to the introduction of differential order λ and integral order μ, the whole controller has two more adjustable parameters, so the setting range of controller parameters becomes larger, the controller can control the controlled object more flexibly, and better control results can be expected. Its transfer function is shown in equation (12) [44]. In order to achieve a trade-off between the complexity and accuracy of the achievable FOPID controller, 5-th order Oustaloup's recursive approximation is done for the integral-differential operators within a chosen frequency band of $\omega \in \{10^{-2}, 10^{2}\}$ rad/s.

$$G_c(s) = K_p + \frac{K_i}{s^{\lambda}} + K_d s^{\mu}, \tag{12}$$

where λ and μ are, respectively, coefficients of integral and differential operators, which are any real numbers, and $\lambda, \mu > 0$.

The fractional-order PID is applied to the parallel PID controller model mentioned above, and the improved

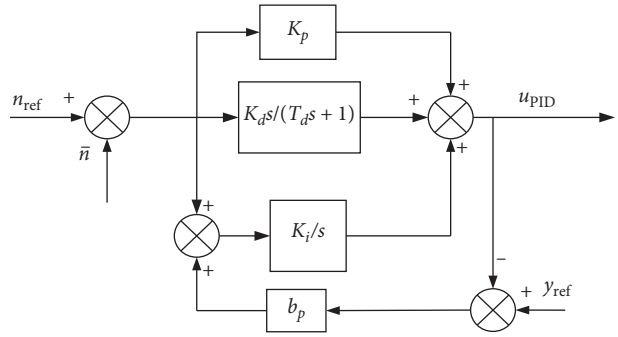

Figure 3: The parallel PID controller.

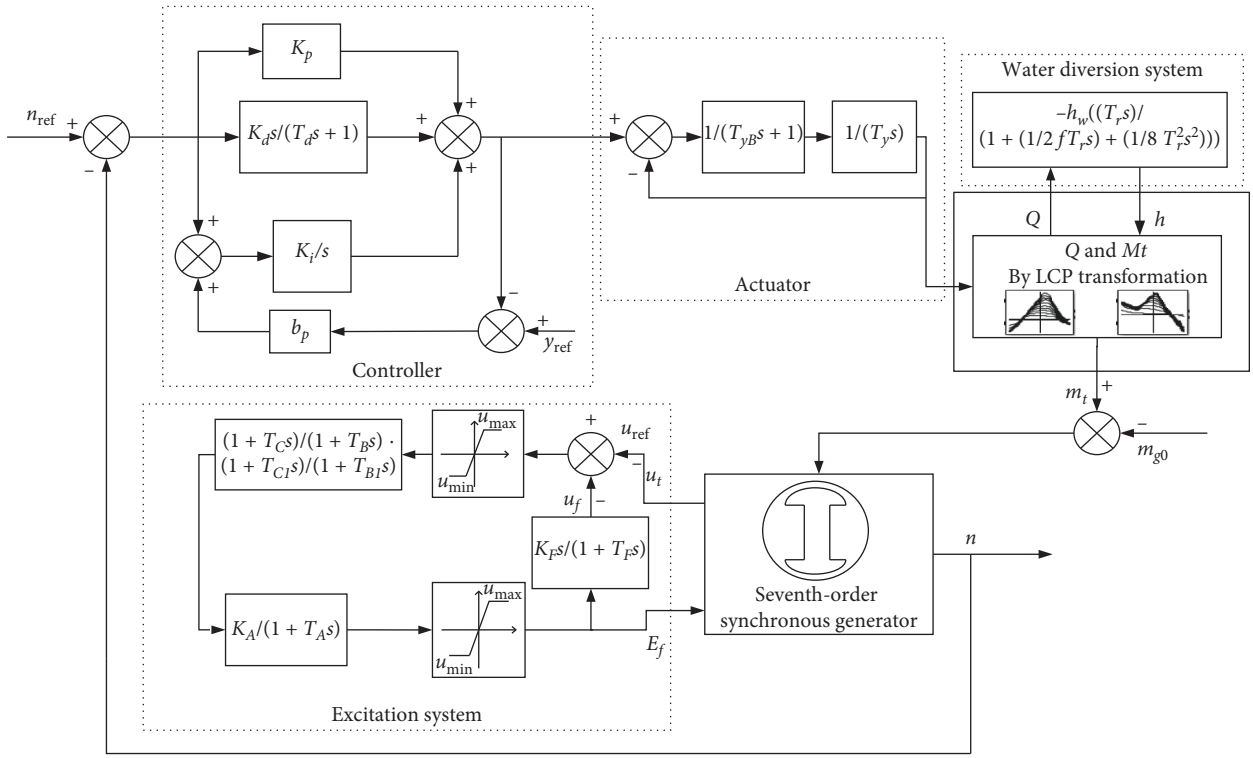

Figure 4: Hydraulic-mechanical-electrical coupling model.

Table 1: Water head and parameters of simulation model of a power station.

Water head (m)			Transfer parameters					
H_{max}	H_r	H_{min}	h_w	T_{yB}	T_y	T_r	k_0	f
217.0	195.0	187.0	1.7	0.02	0.2	1.0	1.0	0.75

Table 2: The set value of guide vane opening at different water heads and loads.

$y_{max} = 43.1^\circ$	H_w (m)			
	190	195	200	210
Opening of 25% load (%)	31	30	27	24
Opening of 50% load (%)	45	42	40	38
Opening of 75% load (%)	64	60	56	52
Opening of 100% load (%)	100	95	90	78

Table 3: The ITAE value of the output frequency ITAE_f when $\Delta f = -0.5$ Hz.

$\Delta f = -0.5$ Hz	H_w (m)			
	190	195	200	210
25% load	0.9065	0.5899	0.6225	0.6025
50% load	0.1527	0.1055	0.1119	0.1217
75% load	0.0649	0.0877	0.0960	0.1031
100% load	0.0032	0.0129	0.0359	0.0429

parallel FOPID governor model is obtained, as shown in Figure 7 [45].

4.2. Proposed Optimization Objective Function. Various time domain integral performance indexes like integral of time

Table 4: The ITAE value of the output frequency ITAE_f when $\Delta f = -0.2$ Hz.

$\Delta f = -0.2$ Hz	H_w (m)			
	190	195	200	210
25% load	0.5666	0.7216	0.8265	0.8966
50% load	0.4498	0.4569	0.4652	0.5117
75% load	0.0751	0.3650	0.4291	0.4525
100% load	0.0209	0.0185	0.0153	0.3211

Table 5: The ITAE value of the output opening ITAE_y when $\Delta f = -0.5$ Hz.

$\Delta f = -0.5$ Hz	H_w (m)			
	190	195	200	210
25% load	0.9041	0.5703	0.6221	0.6276
50% load	0.1764	0.0098	0.1135	0.0099
75% load	0.0084	0.0086	0.0089	0.0092
100% load	0.0061	0.0065	0.0069	0.0075

Table 6: The ITAE value of the output opening ITAE_y when $\Delta f = -0.2$ Hz.

$\Delta f = -0.2$ Hz	H_w (m)			
	190	195	200	210
25% load	0.6971	0.7117	0.7254	0.7436
50% load	0.5992	0.6141	0.6302	0.6453
75% load	0.4548	0.4909	0.5205	0.5497
100% load	0.2023	0.2362	0.2710	0.3643

Table 7: The comprehensive ITAE Index when $\Delta f = -0.5$ Hz.

$\Delta f = -0.5$ Hz	H_w (m)			
	190	195	200	210
25% load	1.8106	1.1603	1.2446	1.2301
50% load	0.3290	0.1153	0.2254	0.1316
75% load	0.0733	0.0963	0.1049	0.1123
100% load	0.0093	0.0194	0.0428	0.0504

Table 8: The comprehensive ITAE Index when $\Delta f = -0.2$ Hz.

$\Delta f = -0.2$ Hz	H_w (m)			
	190	195	200	210
25% load	1.2637	1.4333	1.5519	1.6401
50% load	1.0489	1.0710	1.0954	1.1631
75% load	0.5299	0.8559	0.9495	1.0022
100% load	0.2232	0.2547	0.2863	0.6854

multiplied absolute error (ITAE), integral of time multiplied squared error (ITSE), integral of squared time multiplied error whole squared (ISTES), and integral of squared time multiplied squared error (ISTSE) are considered in the problem similarly, and every index has certain advantages in control system design. For ITAE criterion, time multiplied absolute error of the control system is judged to minimize, and the maximum percentage of overshoot is also minimized since the absolute error is included in the ITAE. The ITSE criterion penalizes the error more than the ITAE, and due to the time multiplication term, the oscillation damps out faster. Other integral performance indexes like ISTES and ISTSE both have higher power of time and error terms. When the pumped storage unit is running under turbine conditions, it mainly is dependent on the parameters of the adjustment device to improve the dynamic quality and stability of the regulation system. ITAE can well express the adjustment speed and depth factors concerned in the optimization of primary frequency regulation parameters. Therefore, in order to improve the dynamic performance of the system after the disturbance is generated, the time domain performance analysis indicators of ITAE is selected in this paper. As shown in equation (13), the weighted structure of the three parameters of water hammer pressure, frequency, and guide vane opening output by the PSURS is adopted. In particular, ITAE values of the three parameters are normalized and weight is redistributed due to their different ranges.

$$J = w_1 \times \text{ITAE\_}h + w_2 \times \text{ITAE\_}y + w_3 \times \text{ITAE\_}f, \quad (13)$$

where ITAE_h, ITAE_y, and ITAE_f are the ITAE values of water hammer pressure, guide vane opening, and frequency, respectively, and w_1, w_2, and w_3 are the weights of the control objective function.

4.3. BCGSA. The GSA is a kind of global optimization algorithm which makes use of the universal gravitation interaction between particles to search intelligently [46]. Premature and falling into local optimum are two common shortcomings of GSA and other swarm intelligence algorithms, which will reduce the accuracy and efficiency of algorithm optimization. The BCGSA introduces P_{best}-G_{best} directed particle update strategy of PSO algorithm, adaptive elastic ball valve boundary processing method, and chemotactic operation in bacterium foraging algorithms (BFA). These three improvement strategies can effectively avoid the algorithm premature and fall into the local optimum and they also can improve the global optimization ability. The advantage of BCGSA for multiparameter optimization has been tested [21].

The computational process of BCGSA algorithm can be summarized as shown in Figure 8. When updating the velocity and position of particles, PSO algorithm's P_{best}-G_{best} oriented particle updating strategy is applied, and the mathematical expressions are shown in equations (14) and (15):

$$v_i^d(t+1) = r_1 \cdot v_i^d(t) + a_i^d(t) + c_1 \cdot r_2 \cdot \left(P_{i\text{best}}^d(t) - x_i^d(t)\right) + c_2 \cdot r_3 \cdot \left(G_{i\text{best}}^d(t) - x_i^d(t)\right), \quad (14)$$

$$x_i^d(t+1) = x_i^d(t) + v_i^d(t), \quad (15)$$

where r_1, r_2, and r_3 are random numbers between [0, 1]; c_1 and c_2 are learning factors whose value range is [0, 2]; $v_i^d(t)$ is the i particle's velocity in the d dimension; $x_i^d(t)$ represents the position of the i particle in the d dimension; $P_{i\text{best}}(t)$ is the

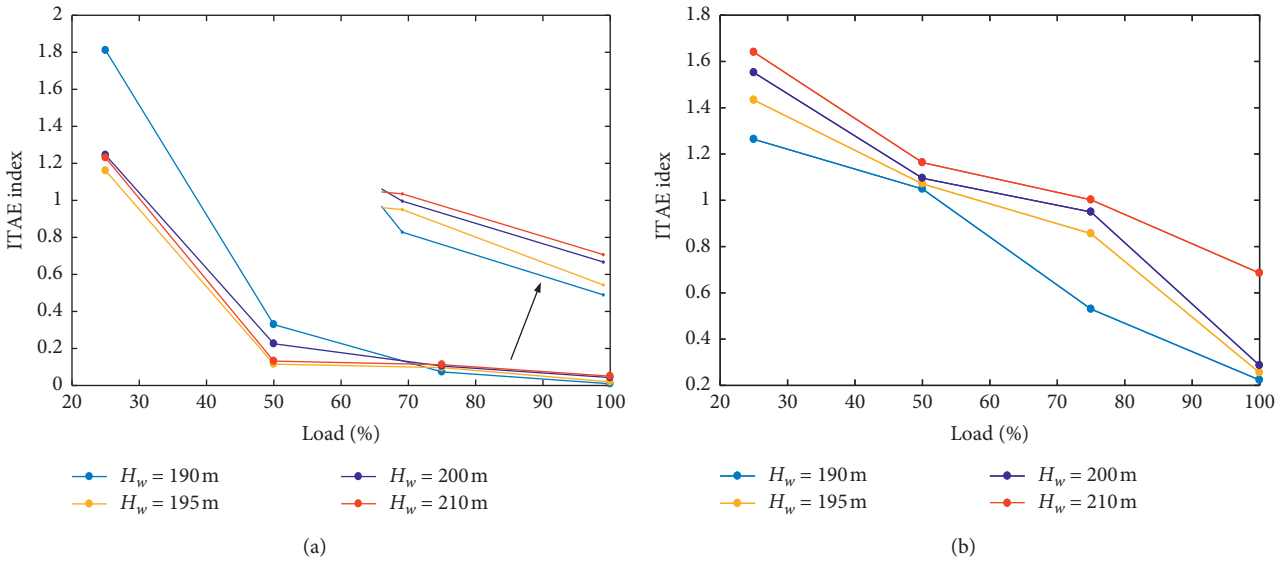

Figure 5: The comprehensive ITAE index of different water heads with different loads. (a) $\Delta f = -0.5$ Hz. (b) $\Delta f = -0.2$ Hz.

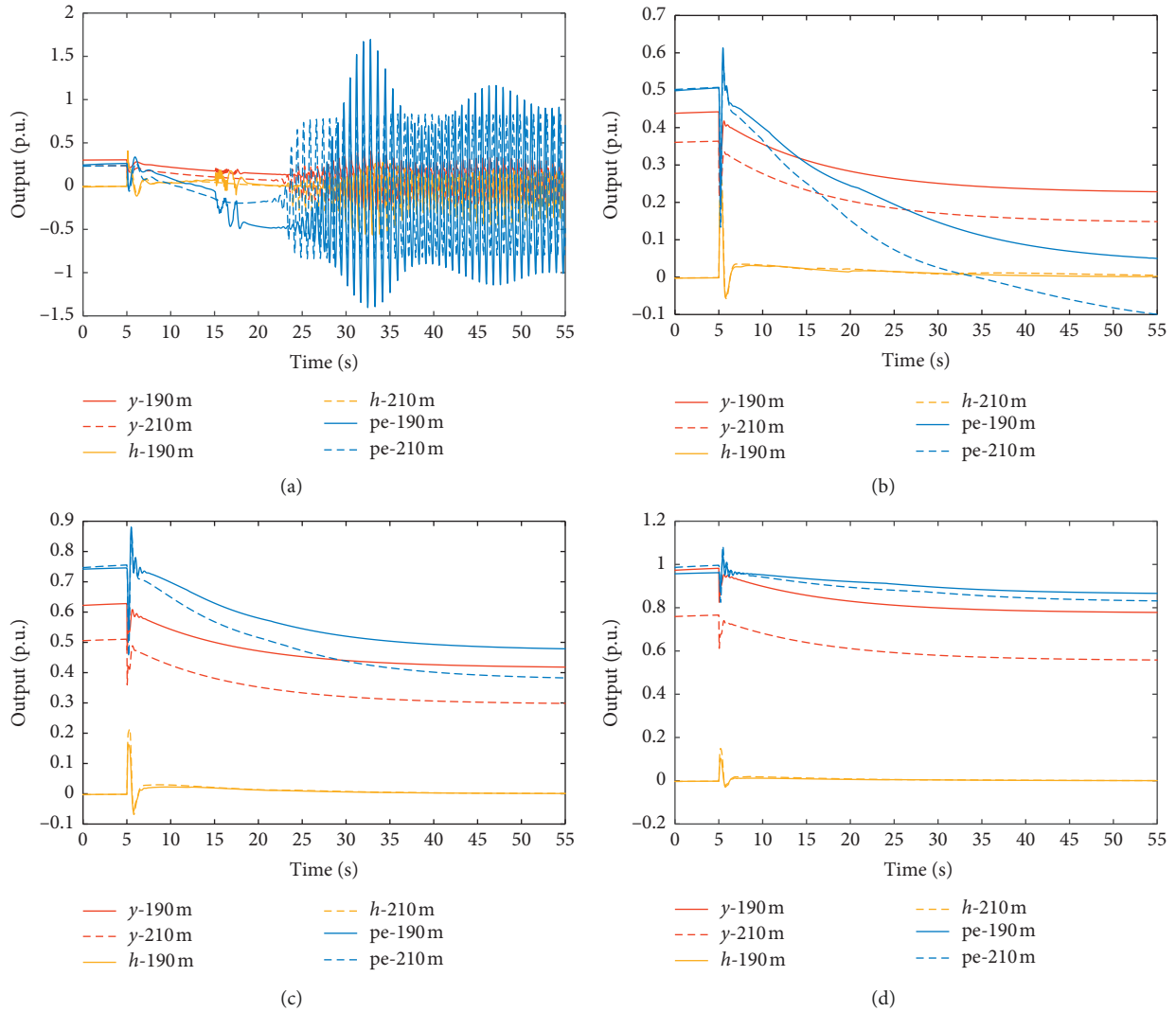

Figure 6: The comparison diagram of y, h, and pe. (a) 25% load. (b) 50% load. (c) 75% load. (d) 100% load.

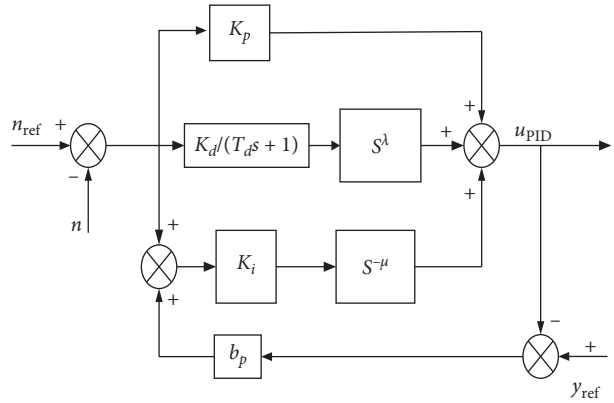

Figure 7: The parallel FOPID controller.

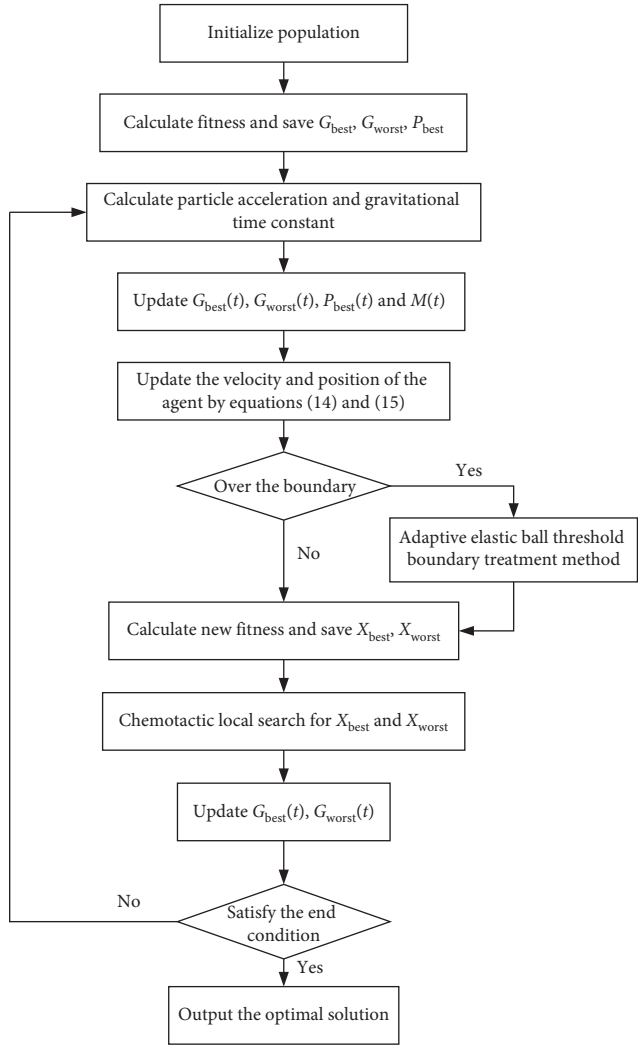

Figure 8: BCGSA optimization steps.

optimal value of the current algebra of the i particle; $G_{\text{best}}(t)$ is the global optimal value of the group; $G_{\text{worst}}(t)$ is the global optimal value of the group; X_{best} is the global optimal particle of the current algebra; and X_{worst} is the global worst particle of the current algebra.

When the velocity and position of each particle are updated, for the particles that cross the threshold boundary, the adaptive pinball method is adopted to process, simulate the bounce characteristics of the elastic ball, and introduce the adaptive elastic coefficient ζ, as shown in the following equation:

$$\begin{cases} \text{if } x_i^d(t) > \text{Ub}(d),\ \text{up} = x_i^d(t) - \text{Ub}(d) \text{ and } x_i^d(t) = \text{Ub}(d) - \zeta \cdot \text{up}, \\ \text{if } x_i^d(t) < \text{Lb}(d),\ \text{down} = \text{Lb}(d) - x_i^d(t) \text{ and } x_i^d(t) = \text{Lb}(d) + \zeta \cdot \text{down}, \end{cases} \tag{16}$$

where Ub(d) and Lb(d) are the upper and lower boundaries of the threshold value of the dimension. For the few particles still clustered at the boundary, their positions will be changed according to the following equation:

$$\begin{aligned} &\text{If } x_i^d(t) > \text{Ub}(d) \text{ or } x_i^d(t) < \text{Lb}(d), \\ &\quad x_i^d(t) = \text{rand} \cdot (\text{Ub}(d) - \text{Lb}(d)) + \text{Lb}(d). \end{aligned} \tag{17}$$

The fitness function value of each particle is calculated, as shown in equations (18) and (19). Chemotaxis local search operation is carried out for global optimal particles and global worst particles of the current algebra according to a certain number of chemotactic steps and moving steps.

$$x(i, j+1) = x(i, j) + C(i)\phi(j), \tag{18}$$

$$\phi(j) = \frac{\Delta(i)}{\sqrt{\Delta^T(i)\Delta(i)}}, \tag{19}$$

where $x(i, j)$ is the position of the ith particle at the jth chemotactic, $C(i)$ is the moving step length after the random direction, $\phi(j)$ is the flipped random direction, and the vector $\Delta(i)$ composed of random number elements between [−1, 1] is randomly generated. Global optimal particle and global worst particle can be updated only when the new particle is better than the original value after the completion of the chemotactic step.

5. Case Study and Analysis

In this section, a comprehensive simulation model of PSURS, which can fully reflect the hydraulic, mechanical, electrical, and other state characteristics of the unit described in Section 2, is built in MATLAB. This paper adopts the actual parameters of a pumped storage power station with a unit capacity of 300 MW in Hubei province, China, which has been applied in practical studies for many times. The traditional PID controller and FOPID controller are, respectively, used in the speed governor part to simulate the control process of the frequency disturbance process under the condition of low water head and small load, and the objective function mentioned in BCGSA and Section 4.2 is used to optimize the control parameters. Furthermore, through comparison with the traditional PID control method, the superiority of the control performance of the selected scheme is verified.

The water head and PSU model parameters of the pumped storage power station are shown in Table 1. It is easy to enter the "S" characteristic area when the unit is running with low water head near the rated water head. Especially in low water head and low water load conditions, the PSU is particularly easy to enter unstable areas when subjected to large frequency disturbances. In this paper, 190 m water head and 25% rated load are selected for the simulation experiment. The population size of BCGSA is 30, and the maximum number of iterations of the algorithm is 100, $c_1 = c_2 = 2$. The control parameters of PSURS are essentially the same as those of the conventional governor. The time range of model simulation is 55 s. PID controller parameter setting range according to relevant regulations and experience is $K_P \in [0.5, 4]$, $K_i \in [0.05, 4]$, and $K_d \in [0.05, 4]$. The adjustment order of the integral order and differential order of FOPID is taken as $\lambda, \mu \in [0.1, 1.1]$.

5.1. Frequency Disturbance of −0.5 Hz under Low Water Head and Small Load Condition. In the control optimization of nonlinear PSURS, when BCGSA is used to set the control parameters of complex time-varying regulation system, the convergence curves of the objective function of the particle swarm optimization (PSO) algorithm, gravitational search algorithm(GSA), and BCGSA are shown in Figure 9. Under the same parameter setting, the overall value of the objective function calculated by BCGSA for the unit optimization controlled by FOPID is lower, and the convergence value is also smaller. According to the convergence curves of PID-PSO, PID- GSA, PID-BCGSA, FOPID-PSO, FOPID- GSA, and FOPID-BCGSA, it is clear that the performance of BCGSA is better than PSO and the standard GSA. It also verifies that the FOPID control effect is generally better than PID control when the unit suffers 0.5 HZ frequency disturbance under the condition of low water head and 25% load.

With reference to the above parameter settings, based on the refined model of PSU, BCGSA is used to optimize the control parameters, and the simulation experiment of frequency disturbance under low water head and small load conditions is carried out. The optimized FOPID and PID control parameters are shown in Table 9. The optimal convergence value of the objective function and the ITAE values of the frequency f, water hammer pressure h, power pe, and guide vane opening y are shown in Table 10. Regulating time t_s and the time t_f at which the output enters violent oscillation of each output are shown in Table 11. t_f is the time when the first wave peak or trough occurs when the output oscillates violently. It can be found from the experiment that there is no significant difference in the length of time when the unit is in a violent oscillation. Therefore, the time when the output enters the first wave peak or trough in the continuous oscillation region is taken as the indicator to consider the regulation effect of PSU. The larger the t_f value is, the slower the unit's response speed to frequency disturbance is, and the smaller the t_f is, the faster the unit's response speed is. t_s is the regulating time in the regional energy index. The transition process curve for each output is shown in Figure 10.

It can be seen from Table 10 that the ITAE values of the output parameters of the unit under the optimal control of

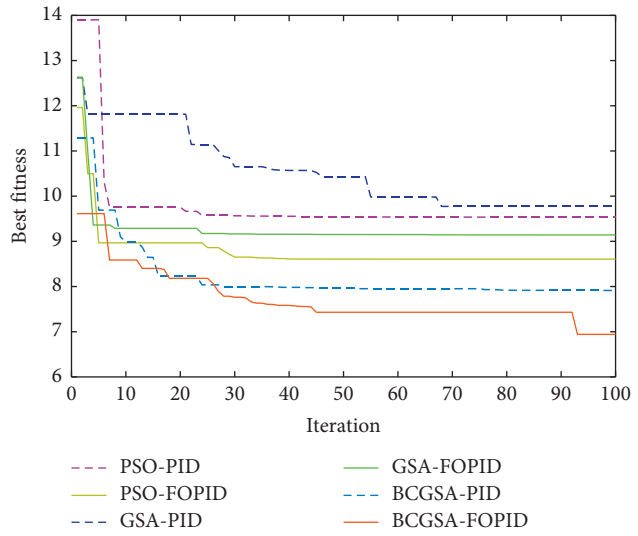

Figure 9: Convergence curves of objective function with $\Delta f = -0.5$ Hz.

Table 9: The optimized controller parameters with $\Delta f = -0.5$ Hz.

Case	Controller parameters				
	K_p	K_i	K_d	λ	μ
PID	3.8507	1.7732	1.2081	—	—
FOPID	2.8946	4.0834	1.7732	0.8049	0.8715

Table 10: Performance indicators with $\Delta f = -0.5$ Hz.

	Index				
	J	ITAE_f	ITAE_h	ITAE_pe	ITAE_y
PID	7.9122	4.1133×10^3	2.9083×10^4	7.0998×10^5	2.2788×10^4
FOPID	6.9413	2.9674×10^3	1.7478×10^4	1.0996×10^5	1.0177×10^4

Table 11: Comparison of performance indexes with $\Delta f = -0.5$ Hz.

Indexes	PID				FOPID			
	f	pe	h	y	f	pe	h	y
$t_f(s)$	15.05	15.12	15.06	15.07	10.42	10.71	10.40	10.53
$t_s(s)$	25.20	43.98	20.03	40.71	17.63	35.56	15.11	30.03

FOPID are relatively small, which effectively improves the regulation quality when the unit suffers from 0.5 Hz frequency disturbance under the condition of low water head and 25% load. The small objective function of FOPID also means that the unit gets good dynamic characteristics. As can be seen from Figure 10 and Table 11, after the disturbance occurs, PSU will still enter the oscillation region, but the frequency of oscillation of the unit under the optimal control of FOPID is reduced, and the t_f value of each parameter is far smaller than that of the unit under PID control, making the oscillation time shorter. The t_s value of the frequency under the control of FOPID is 17.63 s, far less than the 25.20 s under the control of PID, and the frequency is easier to arrive at the stable state. Similarly, the t_s value of the power, water head, and opening degree under the control of FOPID is all less than that of the unit under the control of PID, which indicates that PSU can reach the stable state faster under the control of FOPID. Although the overshoot of FOPID control is slightly larger than that of PID, the dynamic indexes under both controllers meet the requirements of national standards.

5.2. Frequency Disturbance of +0.5 Hz under Low Water Head and Small Load Condition. When frequency disturbance of +0.5 Hz under low water head and small load occurs, different algorithms are used to optimize the controller parameters and the iterative curve of the objective function is shown in Figure 11. On the whole, lower objective function value fully demonstrates the excellent FOPID control with BCGSA under this condition.

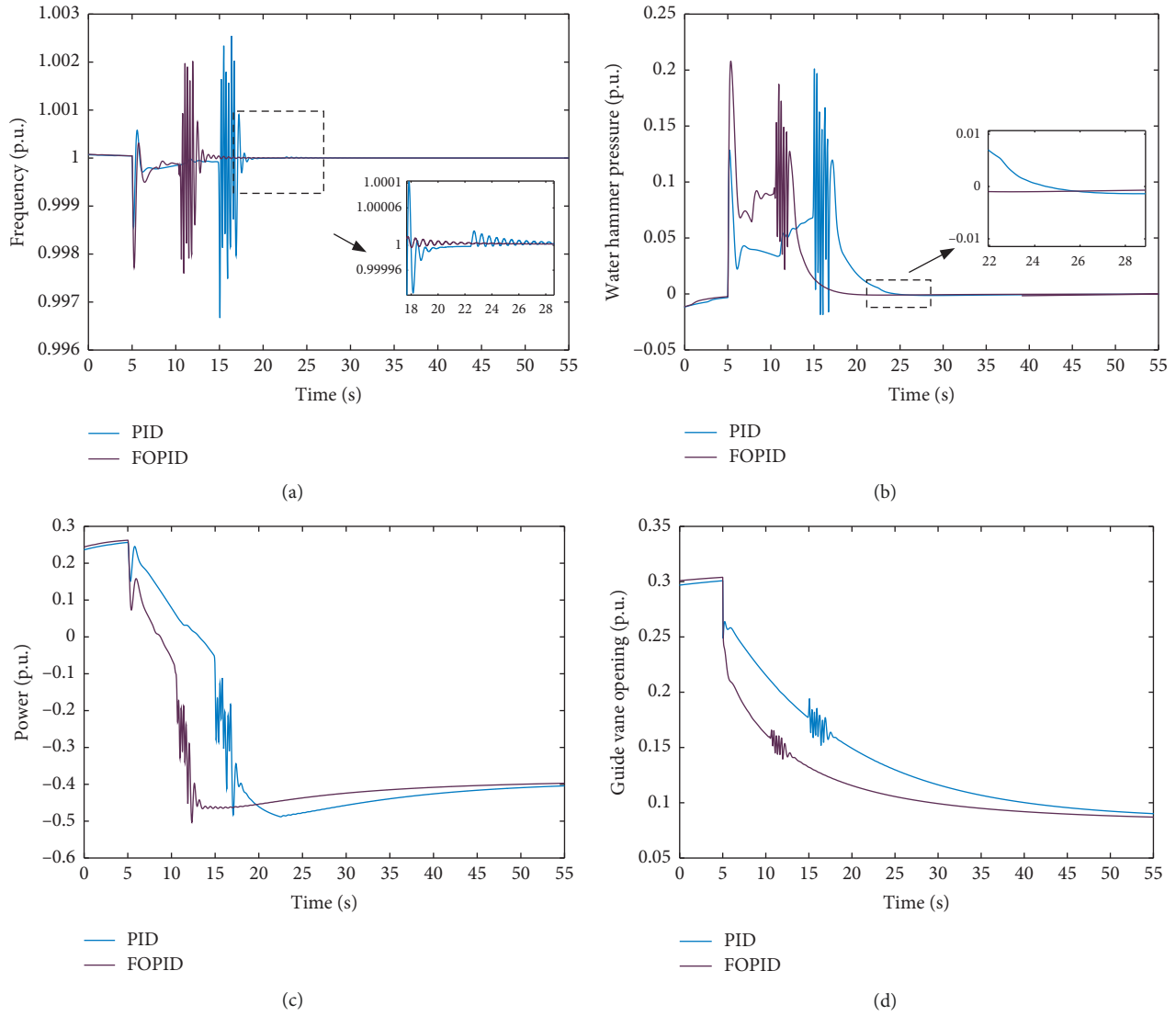

Figure 10: Dynamic response of each output with $\Delta f = -0.5$ Hz. (a) Frequency. (b) Water hammer pressure. (c) Power. (d) Guide vane opening.

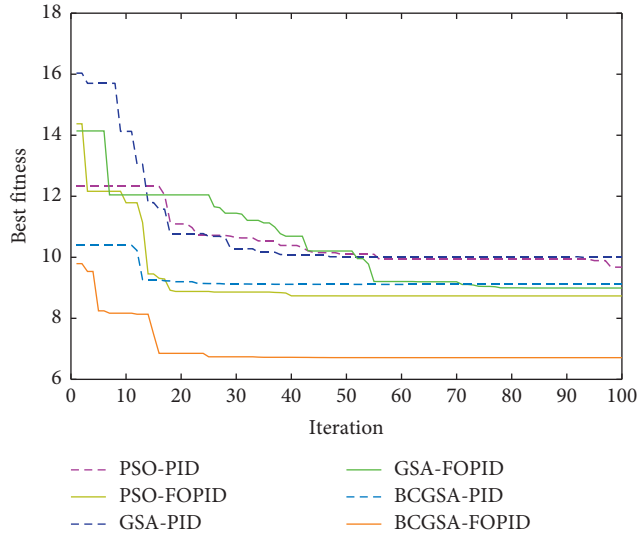

Figure 11: Convergence curves of objective function with $\Delta f = +0.5$ Hz.

Table 12: The optimized controller parameters with $\Delta f = +0.5$ Hz.

Case	Controller parameters				
	K_p	K_i	K_d	λ	μ
PID	3.9992	2.5840	2.4346	—	—
FOPID	2.8370	3.5545	1.5089	1.0007	0.9924

Table 13: Performance indicators with $\Delta f = +0.5$Hz.

	Index				
	J	ITAE_f	ITAE_h	ITAE_pe	ITAE_y
PID	9.1106	81.7019	4.6269×10^3	1.8867×10^4	7.9778×10^3
FOPID	6.7108	76.1314	1.5369×10^3	0.8624×10^4	1.3310×10^3

Table 14: Comparison of performance indexes with $\Delta f = +0.5$ Hz

Indexes	PID				FOPID			
	f	pe	h	y	f	pe	h	y
t_f (s)	11.22	11.10	11.26	11.06	9.942	9.838	10.00	9.950
t_s (s)	15.50	32.87	27.56	42.19	14.12	20.02	22.33	15.56

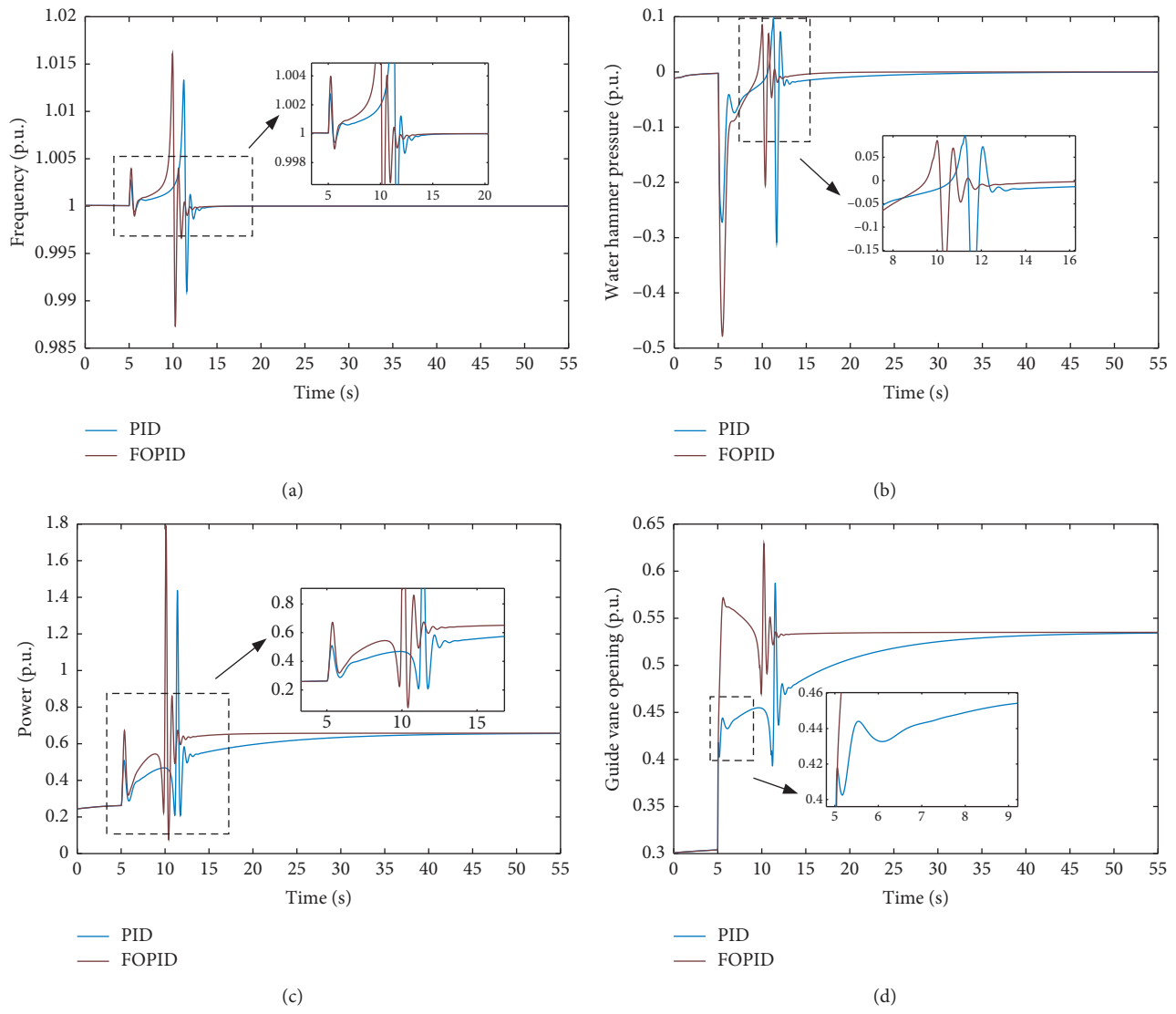

Figure 12: Dynamic response of each output with $\Delta f = +0.5$ Hz. (a) Frequency. (b) Water hammer pressure. (c) Power. (d) Guide vane opening.

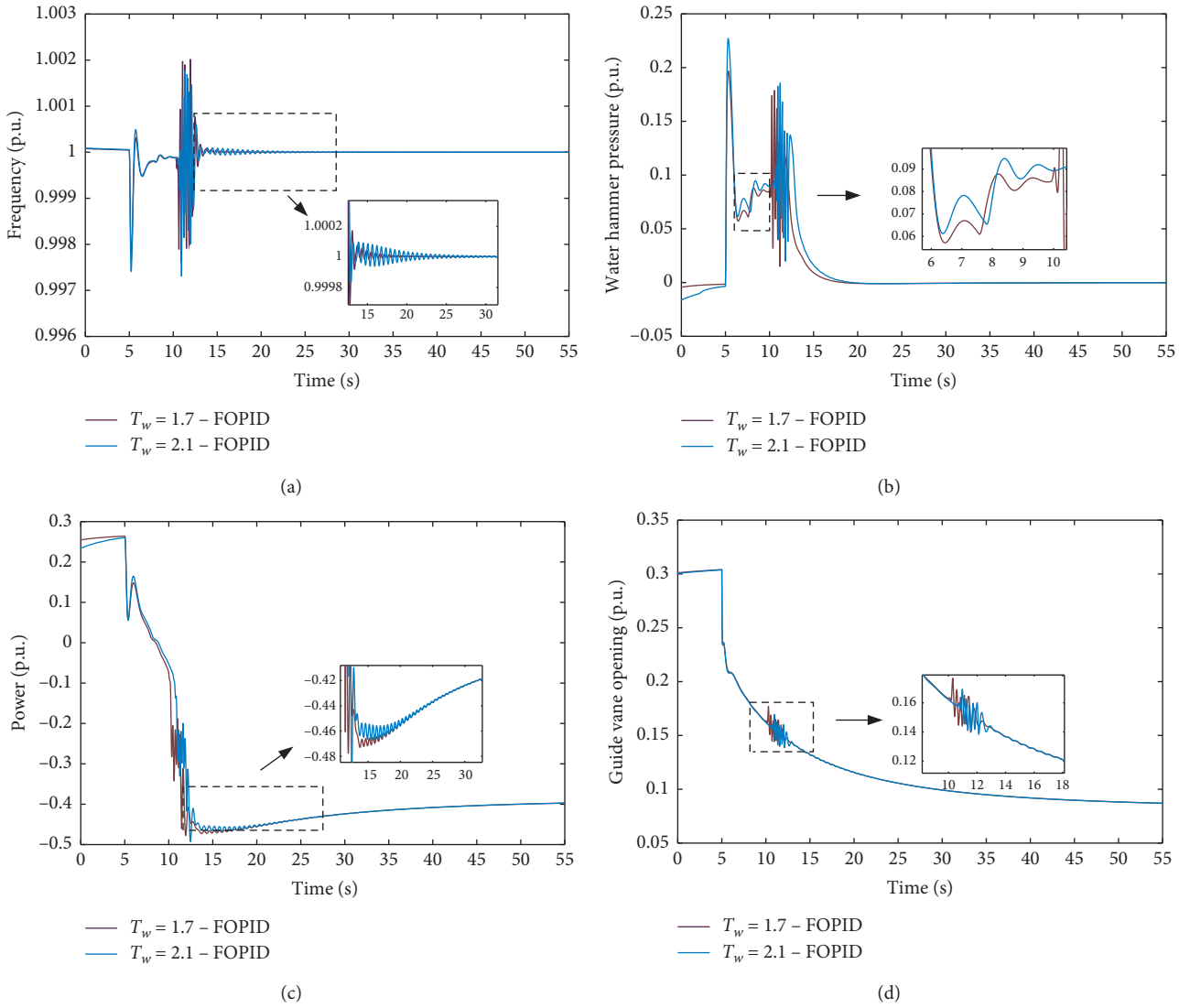

FIGURE 13: Dynamic response of each output at different T_w with $\Delta f = -0.5$ Hz. (a) Frequency. (b) Water hammer pressure. (c) Power. (d) Guide vane opening.

At the same time, the simulation experiment of frequency disturbance of +0.5 Hz under low water head and 25% load is carried out. The optimized control parameters are shown in Table 12, the optimal convergence value of fitness function and the ITAE value of each output are shown in Table 13, the regulating time t_s and the time t_f are shown in Table 14, and the transition process curve of each output is shown in Figure 12.

Similarly, it can be obtained from Table 13 that the ITAE value under FOPID optimization control is smaller, indicating that the dynamic performance of the unit is more excellent at this time. As can be seen from Figure 12 and Table 14, the opening of the pump turbine and the output power of the synchronous generator are particularly rapid in response speed after frequency disturbance. Under the control of FOPID, the t_s value of power is 20.02 seconds, far less than 32.87 s, and the t_s value of the opening is less than half of the PID control. It takes less time for each output to reach the stable state, which indicates that FOPID control has better dynamic characteristics and regulation quality.

5.3. Robustness Analysis of the Obtained Method. The robustness of PSURS is very important for the stable operation of the unit. The PSURS has the function of water diversion system and water flow inertia constant T_w (the value of T_w is $h_w \times T_r$) which is an important factor affecting the dynamic performance of PSURS. Increasing the value of T_w will aggravate the fluctuation of water hammer pressure, which can be used to verify the robustness of the proposed method. Therefore, in the test and experiment of the obtained frequency regulation optimization control method, we adjusted the time constant of water flow inertia constant T_w to be 2.1. The simulation experiment of frequency disturbance of −0.5 Hz under low water head and 25% load is carried out. The dynamic response curve of each output is shown in Figure 13. When T_w increases, the controller and control

parameters in Table 8 are adopted. Compared with T_w of 1.7, the dynamic response process of frequency, water head, power, and opening of the PSURS increases in a small range of amplitude in the oscillation region, but the overall stability time and steady-state error do not change. The optimal primary frequency control method adopted in this paper is robust to the change of hydraulic parameters.

6. Conclusion

For the PSU, when it encounters a large frequency disturbance in the low water head and small load condition, it is easy to enter the unstable region and the oscillation occurs. The characteristic curve of the pump turbine is transformed by LCP, and the PSURS refinement model is established based on the seventh-order synchronous generator with the excitation system. This model can describe the nonlinear relationship between the speed-guide vane opening and the flow and torque, the characteristic of the speed governor's limiting and dead zone, and the complex coupling dynamic response law of the hydraulic-mechanical-electrical system of the regulating system is established. Then, based on the refinement model, the dynamic response characteristics of the PSURS under the condition of primary frequency modulation are analyzed by numerical simulation. The results show that when the unit operates at low water head and 25% load, it suffers from frequency disturbance, and the system is easy to enter the "S" zone and then fall into the state of hydraulic, mechanical, and electrical coupling instability. Therefore, the objective function of control parameter optimization considering hydraulic, mechanical, and electrical factors is established. The FOPID controller is used in the optimization control, and the control parameters are optimized by BCGSA. The simulation results show that the FOPID controller shows strong control performance compared with the traditional PID control when PSURS encounters large frequency disturbance in the low water head and small load condition. It effectively improves the dynamic performance of the unit's transition process. For low water head and small load conditions, the unit has a good inhibitory effect when it encounters a large frequency disturbance and enters an unstable area and violently oscillates.

Nomenclature

h_w: Pipeline characteristic coefficient
T_r: Water hammer pressure wave time constant, s
f: Water head loss coefficient
a: The true value of guide blade opening
n_1: Relative value of unit rotational speed
v_1: Relative value of unit flow
m_1: Relative value of unit torque
v: The voltage, p.u.
i: Current, p.u.
ψ: Flux linkage, p.u.
x_d: Inductance coefficient of d-axis stator winding
x_q: Inductance coefficient of q-axis stator winding
x_f: Inductance coefficient of rotor excitation winding
x_D: Inductance coefficient of d-axis damping winding
x_Q: Inductance coefficient of q-axis damping winding
x_{ad}: Mutual inductance between stator winding and d-axis rotor winding
X_{aq}: Mutual inductance between stator winding and q-axis rotor winding
δ: The load angle, p.u.
H: Inertia constant
ω_0: Rated speed, p.u.
T_m: Active torque, s
K_P: Proportional coefficients
K_i: Integral coefficients
K_d: Differential coefficients
T_d: The time constant of the differential link, s
n_{ref}: The rotational speed relative deviation set value, p.u.
y_{ref}: The guide vane opening relative deviation set value, p.u.
b_p: The perpetual slip coefficient
k_0: Assistant servomotor amplification constant
T_y: Main servomotor response time, s
T_{yB}: Assistant servomotor response time, s
$H_{\max}$: Maximum water head, m
H_r: Rated water head, m
$H_{\min}$: Minimum water head, m.

Data Availability

The data used to support the findings of this study are not available because it involves the parameters and full characteristic data of the actual pumped storage power station.

Conflicts of Interest

The authors declare that they have no conflicts of interest.

Acknowledgments

This work was supported by the National Natural Science Foundation of China (NSFC) (no. 51809099) and Nondestructive Detection and Monitoring Technology for High Speed Transportation Facilities, Key Laboratory of Ministry of Industry and Information Technology (no. KL2019W004).

References

[1] H. Chen, T. N. Cong, W. Yang, C. Tan, Y. Li, and Y. Ding, "Progress in electrical energy storage system: a critical review," *Progress in Natural Science*, vol. 19, no. 3, pp. 291–312, 2009.

[2] W. Fu, K. Wang, C. Li, and J. Tan, "Multi-step short-term wind speed forecasting approach based on multi-scale dominant ingredient chaotic analysis, improved hybrid GWO-SCA optimization and ELM," *Energy Conversion and Management*, vol. 187, pp. 356–377, 2019.

[3] R. Jiang, J. Wang, and Y. Guan, "Robust unit commitment with wind power and pumped storage hydro," *IEEE Transactions on Power Systems*, vol. 27, no. 2, pp. 800–810, 2012.

[4] G. T. Bitew, M. Han, S. A. Mekonnen, S. Patrobers, Z. W. Khan, and L. K. Tuan, "Pumped energy storage system technology and its AC–DC interface topology, modelling and

control analysis: a review," *The Journal of Engineering*, vol. 2019, no. 16, pp. 705–710, 2019.

[5] Z. Zhao, J. Yang, W. Yang, J. Hu, and M. Chen, "A coordinated optimization framework for flexible operation of pumped storage hydropower system: nonlinear modeling, strategy optimization and decision making," *Energy Conversion and Management*, vol. 194, pp. 75–93, 2019.

[6] H. An, J. Yang, W. Yang, Y. Cheng, and Y. Peng, "An improved frequency dead zone with feed-forward control for hydropower units: performance evaluation of primary frequency control," *Energies*, vol. 12, no. 8, p. 1497, 2019.

[7] W. Yang and J. Yang, "Advantage of variable-speed pumped storage plants for mitigating wind power variations: integrated modelling and performance assessment," *Applied Energy*, vol. 237, pp. 720–732, 2019.

[8] G. Zhao and J. Ren, "Research on an output power model of a doubly-fed variable-speed pumped storage unit with switching process," *Applied Sciences*, vol. 9, no. 16, p. 3368, 2019.

[9] L. Meng, H. Wang, and J. S. Tian, "Research on the hydropower frequency control strategy for power delivery grid splitting," *Applied Mechanics and Materials*, vol. 392, pp. 641–645, 2013.

[10] M.-D. Liu, Z. Jia, H.-T. Li, and Y.-C. Cheng, "Hydropower unit primary frequency control model analysis," in *Proceedings of the International Computer Conference on Wavelet Active Media Technology & Information Processing*, Chengdu, China, December 2016.

[11] W. Mo, Y. Chen, H. Chen et al., "Analysis and measures of ultralow-frequency oscillations in a large-scale hydropower transmission system," *IEEE Journal of Emerging and Selected Topics in Power Electronics*, vol. 6, no. 3, pp. 1077–1085, 2018.

[12] D. Zhou, H. Chen, and L. Zhang, "A real-time accurate model and its predictive fuzzy PID controller for pumped storage unit via error compensation," *Energies*, vol. 11, no. 4, p. 35, 2018.

[13] X. Cai, D. Tong, L. Zhang, and J. Cai, "A new governor control algorithm to suppress the pumped-storage unit "S" shape characteristic influence," in *Proceedings of the 2012 24th Chinese Control and Decision Conference (CCDC)*, pp. 2744–2747, Taiyuan, China, May 2012.

[14] S. Q. Zhang, Q. H. Shi, and K. W. Zhang, "Flow behaviour analysis of reversible pump-turbine in "S" characteristic operating zone," *IOP Conference Series: Earth and Environmental Science*, vol. 15, no. 3, Article ID 032045, 2012.

[15] W. Yang, J. Yang, W. Zeng et al., "Experimental investigation of theoretical stability regions for ultra-low frequency oscillations of hydropower generating systems," *Energy*, vol. 186, p. 115816, 2019.

[16] Z. Chen, Y. Yuan, X. Yuan, Y. Huang, X. Li, and W. Li, "Application of multi-objective controller to optimal tuning of PID gains for a hydraulic turbine regulating system using adaptive grid particle swam optimization," *ISA Transactions*, vol. 56, pp. 173–187, 2015.

[17] W. Fu, K. Wang, C. Zhang, and J. Tan, "A hybrid approach for measuring the vibrational trend of hydroelectric unit with enhanced multi-scale chaotic series analysis and optimized least squares support vector machine," *Transactions of the Institute of Measurement and Control*, vol. 41, no. 15, pp. 4436–4449, 2019.

[18] T. V. Plotnikova, P. V. Sokur, P. Y. Tuzov, Y. G. Shakaryan, and M. A. Kuleshov, "Participation of a pumped-storage electric power plant with asynchronous generator-motors in normalized primary frequency regulation," *Power Technology and Engineering*, vol. 49, no. 3, pp. 223–228, 2015.

[19] X. Wu, Y. Xu, J. Liu, C. Lv, J. Zhou, and Q. Zhang, "Characteristics analysis and fuzzy fractional-order PID parameter optimization for primary frequency modulation of a pumped storage unit based on a multi-objective gravitational search algorithm," *Energies*, vol. 13, no. 1, p. 137, 2020.

[20] S. Sondhi and Y. V. Hote, "Fractional order PID controller for load frequency control," *Energy Conversion and Management*, vol. 85, pp. 343–353, 2014.

[21] Y. Xu, J. Zhou, X. Xue, W. Fu, W. Zhu, and C. Li, "An adaptively fast fuzzy fractional order PID control for pumped storage hydro unit using improved gravitational search algorithm," *Energy Conversion and Management*, vol. 111, pp. 67–78, 2016.

[22] Z. Chen, X. Yuan, B. Ji, P. Wang, and H. Tian, "Design of a fractional order PID controller for hydraulic turbine regulating system using chaotic non-dominated sorting genetic algorithm II," *Energy Conversion and Management*, vol. 84, pp. 390–404, 2014.

[23] Y. Tang, M. Cui, C. Hua, L. Li, and Y. Yang, "Optimum design of fractional order PIλDμ controller for AVR system using chaotic ant swarm," *Expert Systems with Applications*, vol. 39, no. 8, pp. 6887–6896, 2012.

[24] C. Zhang, T. Peng, C. Li, W. Fu, X. Xia, and X. Xue, "Multiobjective optimization of a fractional-order PID controller for pumped turbine governing system using an improved NSGA-III algorithm under multiworking conditions," *Complexity*, vol. 2019, p. 18, 2019.

[25] Y. Xu, Y. Zheng, Y. Du, W. Yang, X. Peng, and C. Li, "Adaptive condition predictive-fuzzy PID optimal control of start-up process for pumped storage unit at low head area," *Energy Conversion and Management*, vol. 177, pp. 592–604, 2018.

[26] X. Xia, J. Ji, C.-s. Li, X. Xue, X. Wang, and C. Zhang, "Multiobjective optimal control for hydraulic turbine governing system based on an improved MOGWO algorithm," *Complexity*, vol. 2019, Article ID 3745924, 14 pages, 2019.

[27] O. P. Malik and Y. Zeng, "Design of a robust adaptive controller for a water turbine governing system," *IEEE Transactions on Energy Conversion*, vol. 10, no. 2, pp. 354–359, 1995.

[28] X. Lai, C. Li, J. Zhou, and N. Zhang, "Multi-objective optimization of the closure law of guide vanes for pumped storage units," *Renewable Energy*, vol. 139, pp. 302–312, 2019.

[29] Y. Zhang, J. Zhou, Y. Zheng, and Y. Xu, "Control optimisation for pumped storage unit in micro-grid with wind power penetration using improved grey wolf optimiser," *IET Generation, Transmission & Distribution*, vol. 11, no. 13, pp. 3246–3256, 2017.

[30] E. Rashedi, H. Nezamabadi-Pour, and S. Saryazdi, "GSA: a gravitational search algorithm," *Information Sciences*, vol. 179, no. 13, pp. 2232–2248, 2009.

[31] C. Li, J. Zhou, B. Fu, P. Kou, and J. Xiao, "T–S fuzzy model identification with a gravitational search-based hyperplane clustering algorithm," *IEEE Transactions on Fuzzy Systems*, vol. 20, no. 2, pp. 305–317, 2012.

[32] R. D. Fard, M. Karrari, and O. P. Malik, "Synchronous generator model identification for control application using volterra series," *IEEE Transactions on Energy Conversion*, vol. 20, no. 4, pp. 852–858, 2005.

[33] A. S. Kocaman and V. Modi, "Value of pumped hydro storage in a hybrid energy generation and allocation system," *Applied Energy*, vol. 205, pp. 1202–1215, 2017.

[34] Z. Li and O. P. Malik, "An orthogonal test approach based control parameter optimization and its application to a hydro-turbine governor," *IEEE Transactions on Energy Conversion*, vol. 12, no. 4, pp. 388–393, 1997.

[35] I. Chalghoum, S. Elaoud, M. Akrout, and E. H. Taieb, "Transient behavior of a centrifugal pump during starting period," *Applied Acoustics*, vol. 109, pp. 82–89, 2016.

[36] Y. Xu, J. Zhou, Y. Zhang, W. Fu, and X. Zhang, "Parameter optimization of robust non-fragile fractional order PID controller for pump turbine governing system," in *Proceedings of the Sixth International Conference on Instrumentation & Measurement*, pp. 15–18, Harbin, China, July 2016.

[37] M. Dehghani and M. Karrari, "Nonlinear robust modeling of synchronous generators," *Iranian Journal of Science and Technology Transaction B-Engineering*, vol. 31, pp. 629–640, 2007.

[38] N. Jiang and H.-D. Chiang, "A two-time scale dynamic correction method for fifth-order generator model undergoing large disturbances," *IEEE Transactions on Power Systems*, vol. 31, no. 5, pp. 3616–3623, 2016.

[39] I. M. Canay, "Determination of model parameters of synchronous machines," *IEEE Proceedings Part B: Electric Power Applications*, vol. 130, no. 2, pp. 86–94, 2008.

[40] N. Jiang and H.-D. Chiang, "Damping representation for the fifth-order generator model in transient behaviors," *IEEE Transactions on Power Systems*, vol. 32, no. 6, pp. 4924–4933, 2017.

[41] L. M. Hajagos and M. J. Basler, "Changes to IEEE 421.5 recommended practice for excitation system models for power system stability studies," in *Proceedings of the IEEE Power Engineering Society General Meeting*, San Francisco, CA, USA, June 2005.

[42] Y. Xu, C. Li, Z. Wang, N. Zhang, and B. Peng, "Load frequency control of a novel renewable energy integrated micro-grid containing pumped hydropower energy storage," *IEEE Access*, vol. 6, pp. 29067–29077, 2018.

[43] L. Liu and S. Zhang, "Robust fractional-order PID controller tuning based on bode's optimal loop shaping," *Complexity*, vol. 2018, Article ID 6570560, 14 pages, 2018.

[44] I. Pan and S. Das, "Frequency domain design of fractional order PID controller for AVR system using chaotic multi-objective optimization," *International Journal of Electrical Power & Energy Systems*, vol. 51, pp. 106–118, 2013.

[45] C. Li, N. Zhang, X. Lai, J. Zhou, and Y. Xu, "Design of a fractional-order PID controller for a pumped storage unit using a gravitational search algorithm based on the Cauchy and Gaussian mutation," *Information Sciences*, vol. 396, pp. 162–181, 2017.

[46] C. Li and J. Zhou, "Semi-supervised weighted kernel clustering based on gravitational search for fault diagnosis," *ISA Transactions*, vol. 53, no. 5, pp. 1534–1543, 2014.